# Generalizable neural-network parameterization of mesoscale eddies in idealized and global ocean models

**Pavel Perezhogin[1], Alistair Adcroft[3], Laure Zanna[1,2]**

[1]Courant Institute of Mathematical Sciences, New York University, New York, NY, USA
[2]Center for Data Science, New York University, New York, NY, USA
[3]Program in Atmospheric and Oceanic Sciences, Princeton University, Princeton, NJ, USA

**Key Points:**

- Physics constraints are developed for the neural-network parameterization of mesoscale eddy fluxes
- Constraint for dimensional scaling improves offline generalization to unseen grid resolutions and depths
- New parameterization improves the representation of kinetic and potential energy online in coarse idealized and global ocean models

Corresponding author: Pavel Perezhogin, pp2681@nyu.edu

**Abstract**
Data-driven methods have become popular to parameterize the effects of mesoscale eddies in ocean models. However, they perform poorly in generalization tasks and may require retuning if the grid resolution or ocean configuration changes. We address the generalization problem by enforcing physical constraints on a neural network parameterization of mesoscale eddy fluxes. We found that the local scaling of input and output features helps to generalize to unseen grid resolutions and depths offline in the global ocean. The scaling is based on dimensional analysis and incorporates grid spacing as a length scale. We formulate our findings as a general algorithm that can be used to enforce data-driven parameterizations with dimensional scaling. The new parameterization improves the representation of kinetic and potential energy in online simulations with idealized and global ocean models. Comparison to baseline parameterizations and impact on global ocean biases are discussed.

## Plain Language Summary

Ocean models can't directly simulate eddies that are smaller than the resolution of the computational grid. The effect of these eddies is represented by parameterizations. Machine learning offers a new way to build parameterizations directly from data, however, such parameterizations may fail when tested in new, unseen scenarios. Here, we leverage physics constraints to mitigate this, generalization, problem. Specifically, we found that method of dimensional analysis can be used to constrain data-driven parameterizations to enhance their accuracy in new scenarios without the need for retraining. New parameterization is tested in a realistic ocean model and brings us closer to robust, data-driven methods for ocean and climate models.

## 1 Introduction

Numerical ocean models rely on parameterizations to represent the effects of physical processes smaller than the model grid spacing, which are unresolved (Fox-Kemper et al., 2019; Hewitt et al., 2020; Christensen & Zanna, 2022). Recently, there has been a growing interest in applying machine learning methods to parameterize these subgrid physics in ocean models (Bolton & Zanna, 2019; Zanna & Bolton, 2020; Guillaumin & Zanna, 2021; Zhang et al., 2023; Sane et al., 2023; Yan et al., 2024; Perezhogin, Zhang, et al., 2024; Maddison, 2024). However, developing data-driven parameterizations for ocean models is still in its early stages, and their application is often limited to idealized configurations. Deploying data-driven parameterizations in the global ocean presents several challenges, one of which is addressed in this study – the problem of generalization to unseen scenarios.

Data-driven parameterizations rely heavily on sets of training data, and their successful implementation often requires tuning when applied to a new grid resolution (Zhang et al., 2023), flow regime (Ross et al., 2023), model configuration (Perezhogin, Zhang, et al., 2024), depth, or geographical region (Gultekin et al., 2024). However, in practice, it would be desirable to have a single parameterization that performs effectively across a variety of scenarios without requiring retuning. The ability of a data-driven model to work on new (testing) data, which is distinct from the training data, is measured by the *generalization error* (Bishop & Nasrabadi, 2006; Hastie et al., 2009). Data-driven methods work best when the testing data is drawn from the same distribution as the training data. However, in geophysical applications, the distribution of physical variables can vary vastly across different scenarios—a phenomenon referred to as a *distribution shift* (Beucler et al., 2024; Gultekin et al., 2024). In this case, domain knowledge and physics constraints can be leveraged to mitigate the generalization error of data-driven models (Kashinath et al., 2021).

In this work, we demonstrate how physics constraints can be leveraged to enhance the generalization of an Artificial Neural Network (ANN) parameterization of the ocean mesoscale eddy fluxes. Following Beucler et al. (2024), we rescale features of the ANN to minimize the distribution shift. To identify a suitable normalization technique for eddy fluxes, we apply dimensional analysis and Buckingham (1914)'s Pi theorem. Specifically, we introduce a local dimensional scaling constructed from the grid spacing and velocity gradients (Prakash et al., 2022). The local scaling improves offline generalization of the ANN parameterization to unseen grid resolutions and depths, as found in the global ocean dataset CM2.6 (Griffies et al., 2015). Our findings are formulated as a general algorithm that can be used to incorporate the dimensional scaling in future applications. Additional physics constraints for the ANN parameterization are enforced following Guan et al. (2022) and Srinivasan et al. (2024). We present an online evaluation of the new ANN parameterization in the GFDL MOM6 ocean model (Adcroft et al., 2019) in idealized and global configurations.

## 2 A Method to Constrain Neural Network with Dimensional Scaling

Here we introduce the concept of physical dimensionality and demonstrate how it can be used to constrain data-driven parameterizations. We start with a trivial example, followed by a general algorithm. Finally, we draw connections to existing approaches.

### 2.1 Trivial Example

Consider the case where a scalar momentum flux $T$ (units of $\mathrm{m}^2\mathrm{s}^{-2}$) can be predicted using a length scale $\Delta$ (units of m) and inverse time scale $X$ (units of $\mathrm{s}^{-1}$):

$$T = f(\Delta, X). \tag{1}$$

Eq. (1) must remain invariant under rescaling the units of time and length, that is for any $\alpha, \beta > 0$, the equality must hold: $f(\alpha\Delta, \beta X) = \alpha^2\beta^2 f(\Delta, X)$. However, the unit invariance can be violated when $f$ is parameterized by neural networks. One way to enforce it is by leveraging Buckingham (1914)'s Pi theorem, which states that the dimensional equation (such as Eq. (1)) can be rewritten in non-dimensional form. Specifically, for a set of three dimensional variables ($T$, $\Delta$, $X$) with two independent dimensions (length and time), there is only one (three minus two) non-dimensional variable ($\pi_1 = T/(\Delta^2 X^2)$). Thus, Eq. (1) transforms to $\pi_1 = \text{const}$, or equivalently:

$$T = \Delta^2 X^2 \theta, \tag{2}$$

where $\theta$ can be interpreted as a non-dimensional Smagorinsky (1963) coefficient. A data-driven parameterization in the form of Eq. (2) with a trainable parameter $\theta$, which is constant, follows the dimensional scaling as a hard constraint, in contrast to Eq. (1), which does not guarantee dimensional consistency. Eq. (2) promotes generalization as it explicitly accounts for the change in the magnitude of independent variables ($\Delta$ and $X$), constraining the learnable part of the mapping ($\theta$) to be on the order of unity.

### 2.2 General Algorithm

Extending the example above, we suggest an algorithm to enforce dimensional scaling in ANN parameterizations by preprocessing input and output features:

1. Identify the input features that contribute significantly to the accurate prediction of the output features;
2. Construct non-dimensional input and output features from a *combined* set of identified input and output features;
3. Verify that a traditional known parameterization is a special case of the constructed non-dimensional mapping.

Step 1 follows standard dimensional analysis textbooks (Bridgman, 1922; Barenblatt, 1996). Specifically, a relevant set of input features can be identified by physical intuition or through ablation studies by evaluating the gain in offline performance from including additional dimensional features in the input set. Constructing non-dimensional features is a common approach in physics-constrained data-driven parameterizations (Ling et al., 2016; Schneider et al., 2024). However, the normalization of input features is often considered separately from the normalization of output features (Xie et al., 2020; Kang et al., 2023; Beucler et al., 2024; Christopoulos et al., 2024), unlike our proposed method (step 2 above). Additionally, the emphasis in these works is often placed on identifying normalization factors that minimize the distribution shift, while we suggest starting with identifying features responsible for the prediction (step 1). Finally, traditional parameterizations are often used to propose efficient normalization factors (Xie et al., 2020; Kang et al., 2023; Connolly et al., 2025), while we instead advocate for having traditional parameterizations as a special case (step 3, Prakash et al. (2022, 2024)).

## 3 Physics Constraints for Ocean Mesoscale Parameterization

Our goal is to predict the subfilter momentum fluxes of mesoscale eddies using an Artificial Neural Network (ANN) parameterization, see schematic in Figure 1(a). Various physical invariances were imposed to promote generalization.

### 3.1 Learning Subfilter Fluxes

We consider the acceleration produced by subfilter ocean mesoscale eddies (subfilter forcing, Bolton & Zanna, 2019):

$$\partial_t \overline{\mathbf{u}} = \mathbf{S} = (\overline{\mathbf{u}} \cdot \nabla)\overline{\mathbf{u}} - \overline{(\mathbf{u} \cdot \nabla)\mathbf{u}}, \tag{3}$$

where $\mathbf{u} = (u, v)$ is the horizontal ocean velocity, $\nabla = (\partial_x, \partial_y)$ is the horizontal gradient, and $\overline{(\cdot)}$ is the horizontal filter. The subfilter forcing can be approximated (Loose, Marques, et al., 2023) as a divergence of the momentum flux:

$$\mathbf{S} \approx \nabla \cdot \mathbf{T} \tag{4}$$

where

$$\mathbf{T} = \begin{pmatrix} T_{xx} & T_{xy} \\ T_{xy} & T_{yy} \end{pmatrix} = \begin{pmatrix} \overline{u}\,\overline{u} - \overline{uu} & \overline{u}\,\overline{v} - \overline{uv} \\ \overline{u}\,\overline{v} - \overline{uv} & \overline{v}\,\overline{v} - \overline{vv} \end{pmatrix}. \tag{5}$$

We predict the three components of $\mathbf{T}$, namely $T_{xx}$, $T_{xy}$, $T_{yy}$, similarly to Zanna and Bolton (2020) (ZB20 hereafter) to (i) impose momentum conservation as a hard constraint, (ii) enforce symmetry of the tensor, which leads to angular momentum conservation (Griffies, 2018, Section 17.3.3).

We learn the components of $\mathbf{T}$ by minimizing the mean squared error (MSE) loss function:

$$\mathcal{L}_{\text{MSE}} = ||(\mathbf{S} - \nabla \cdot \widehat{\mathbf{T}}) \cdot m||_2^2 \;/\; ||\mathbf{S} \cdot m||_2^2, \tag{6}$$

where $m$ is the mask of wet points and $\widehat{\mathbf{T}} \equiv \widehat{\mathbf{T}}(\mathbf{X})$ is the prediction of the subfilter flux with $\mathbf{X}$ being the vector of input features discussed below. See SI for further details.

### 3.2 Input Features

Following ZB20, we consider the components of the strain-rate tensor and vorticity as input features for prediction:

$$\begin{aligned} \overline{\sigma}_S &= \partial_y \overline{u} + \partial_x \overline{v} && \text{– shearing strain,} \\ \overline{\sigma}_T &= \partial_x \overline{u} - \partial_y \overline{v} && \text{– horizontal tension/stretch,} \\ \overline{\omega} &= \partial_x \overline{v} - \partial_y \overline{u} && \text{– relative vorticity.} \end{aligned} \tag{7}$$

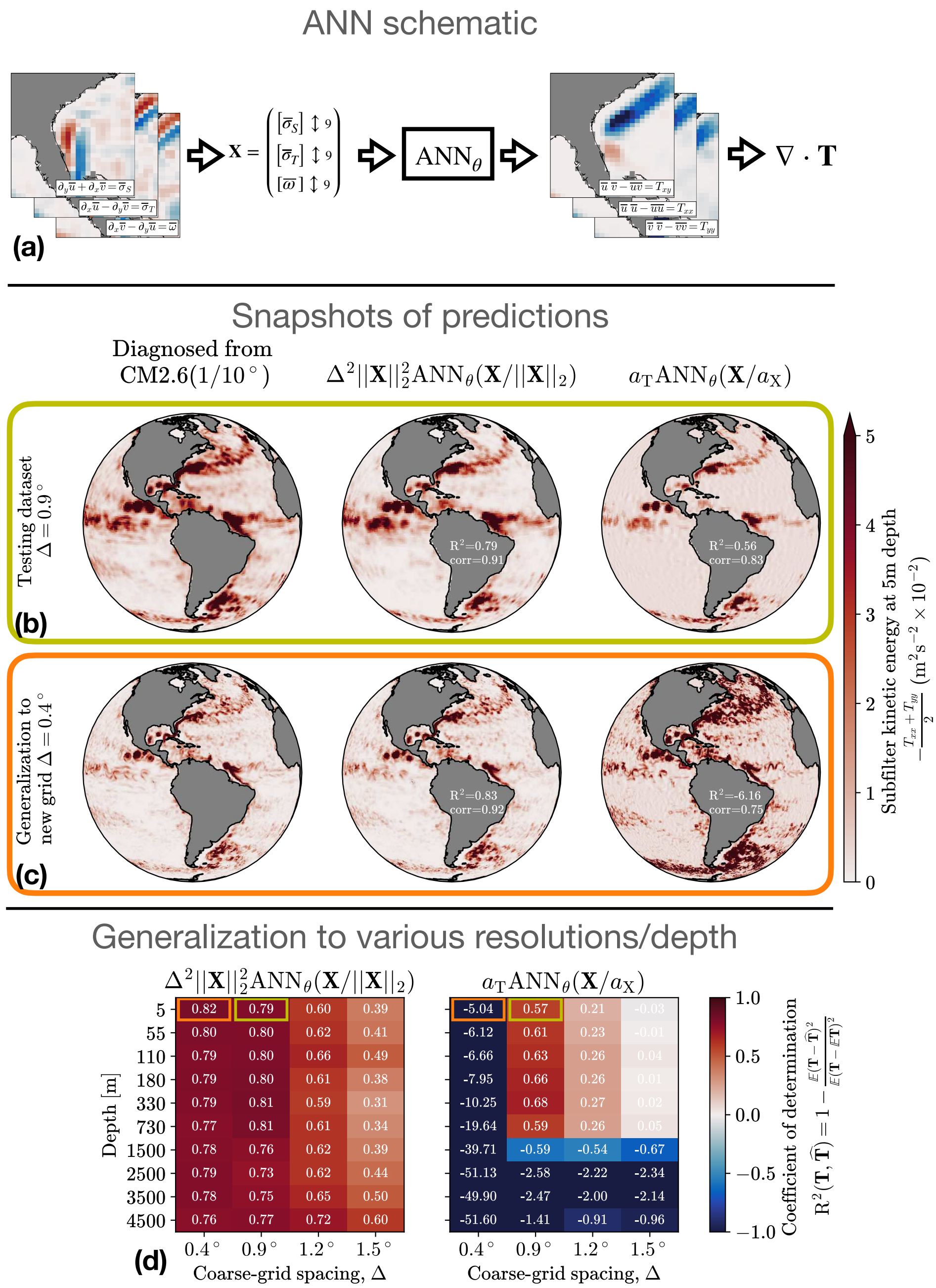


**Figure 1.** (a) Artificial neural network (ANN) parameterization predicting the subfilter fluxes given the velocity gradients on the horizontal stencil of 3×3 points. (b) Snapshots of predictions by two ANNs: with local dimensional scaling (Eq. (11), center column) or with fixed normalization coefficients (Eq. (9), right column) at the resolution (0.9°) and depth (5m) used for training (testing data is separated by 10 years). (c) Prediction at the unseen resolution (0.4°) and the same depth (5m). (d) Coefficient of determination ($R^2$) in prediction of subfilter fluxes for various resolutions and depths, different from that used for training (0.9°, 5m). The $R^2$ is averaged over 2 years of held-out data and excludes 2 grid points adjacent to the coastline, where green and orange boxes correspond to panels (b) and (c), respectively.

These input features exclude explicit dependence on the velocity, guaranteeing Galilean invariance of the parameterization (Srinivasan et al., 2024; Pope, 1975; Lund & Novikov, 1993; Ling et al., 2016). When using the input features (Eq. (7)) pointwise, the resulting ANN parameterization highly correlates with the ZB20 equation-discovery model. Thus, we decided to include the non-local contribution of these features (Srinivasan et al., 2024). To do so, the input vector to the ANN consists of velocity gradients, each defined on a 3 × 3 horizontal stencil and flattened into a vector of length 9 (denoted as $[\cdot]\updownarrow_9$):

$$\mathbf{X} = \begin{pmatrix} [\overline{\sigma}_S]\updownarrow_9 \\ [\overline{\sigma}_T]\updownarrow_9 \\ [\overline{\omega}]\updownarrow_9 \end{pmatrix} \in \mathbb{R}^{27}. \tag{8}$$

Including information about velocity gradients from the closest neighboring points is a common approach in subgrid modeling (Maulik & San, 2017; Maulik et al., 2019; Pawar et al., 2020; Wang et al., 2021, 2022; Gultekin et al., 2024).

### 3.3 Neural Network Parameterizations

We consider a baseline data-driven parameterization of eddy fluxes with fixed normalization coefficients:

$$\mathbf{T} \approx \widehat{\mathbf{T}}(\mathbf{X}) = a_{\mathrm{T}}\mathrm{ANN}_\theta(\mathbf{X}/a_{\mathrm{X}}), \tag{9}$$

where $\mathrm{ANN}_\theta$ is the neural network with trainable parameters $\theta$, $\mathbf{X}$ is the input features (Eq. (8)), and coefficients $a_{\mathrm{T}} = 10^{-2}\mathrm{m}^2\mathrm{s}^{-2}$ and $a_{\mathrm{X}} = 10^{-6}\mathrm{s}^{-1}$ approximate the standard deviations of eddy fluxes and velocity gradients in our dataset. Using fixed normalization coefficients in parameterizations similar to Eq. (9) is a common practice (Srinivasan et al., 2024). Below, we contrast this approach to a normalization that follows solely from dimensional analysis presented in Section 2.

To facilitate generalization across different resolutions of the coarse grid (scale-aware or grid-aware parameterization, Bachman et al., 2017), we include the grid spacing of the coarse model $\Delta = \sqrt{\Delta x \Delta y}$ to a set of input features (Lund & Novikov, 1993; Li et al., 2025):

$$\mathbf{T} \approx \widehat{\mathbf{T}}(\mathbf{X}, \Delta). \tag{10}$$

Including grid spacing is physically justified as velocity gradients and momentum fluxes differ in dimensionality and require a length scale to be invoked.

Finally, we enforce parameterization given in Eq. (10) with the dimensional scaling. A combined set of input and output features ($\mathbf{T}$, $\mathbf{X}$, $\Delta$) is used to construct non-dimensional input ($\mathbf{X}/||\mathbf{X}||_2$) and output ($\mathbf{T}/(\Delta||\mathbf{X}||_2)^2$) features, where $||\mathbf{X}||_2 = \sqrt{\sum_i X_i^2}$. This normalization of features is local, that is computed separately for each grid point. By designing the ANN to operate on non-dimensional variables, we propose a parameterization with the local dimensional scaling (Reissmann et al., 2021; Prakash et al., 2022):

$$\widehat{\mathbf{T}}(\mathbf{X}, \Delta) = \Delta^2||\mathbf{X}||_2^2\mathrm{ANN}_\theta(\mathbf{X}/||\mathbf{X}||_2). \tag{11}$$

According to the Buckingham (1914)'s Pi theorem, there is freedom in constructing non-dimensional variables. We opt to use the non-dimensional vector $\mathbf{X}/||\mathbf{X}||_2$ to constrain the range of its components between $-1$ and 1, thereby reducing the distribution shift in ANN inputs. The model form (Eq. (11)) admits ZB20, Smagorinsky, biharmonic Smagorinsky, and Leith (1996) parameterizations as special cases, with well-behaved functional representations, see Text S1 in SI for details.

### 3.4 Summary on Physics Constraints

Parameterization in Eq. (11) encapsulates conservation of momentum, angular momentum, Galilean invariance, and local dimensional scaling. In addition, we also independently rotate the training snapshots by 90° degrees, and reflect them along $x$ and $y$

axes, creating $8 = 2^3$ training snapshots from one snapshot to promote rotational and reflection invariances via data augmentation (Guan et al., 2022).

## 4 Results

### 4.1 Training and offline generalization

We train ANNs to predict the divergence of subfilter fluxes (Eq. (6)) using filtered velocity gradients (Eq. (7)) as input features. Our main goal is to demonstrate that the local dimensional scaling promotes the generalization to unseen grid resolutions and depths. Limited generalization in such scenarios has been reported for previous machine-learning models of mesoscale eddies (Zhang et al., 2023; Gultekin et al., 2024; Ross et al., 2023) and traditional physics-based parameterizations (Yankovsky et al., 2024). The training dataset is created using the climate model CM2.6 (Griffies et al., 2015) with a 0.1° ocean component. Input and output features are diagnosed by filtering and coarse-graining the climate model data. The filtering is Gaussian (Grooms et al., 2021) with a filter width three times the coarse grid spacing. See Text S2 and Table S1 in SI for details.

We compare two ANNs: one incorporating local dimensional scaling (Eq. (11)) and a baseline ANN with fixed normalization coefficients (Eq. (9)). Both ANNs are very small and have only one hidden layer with 20 neurons, chosen to fit the ANN inference time within 10% of ocean model runtime (see Texts S2 and S3 in SI). To explore generalization, we let the ANNs learn based solely on data from one combination of depth (5m) and coarse grid spacing (0.9°) during training. The offline evaluation of ANNs on held-out data similar to that used for training is shown in Figure 1(b). Since there is no distribution shift between training and testing data, the baseline ANN demonstrates reasonably high pattern correlation (0.83) and $\mathrm{R}^2$ (0.56) in the prediction of subfilter fluxes. Incorporating the local dimensional scaling improves the pattern correlation (0.91) and $\mathrm{R}^2$ (0.79) due to the latitudinal dependence of the grid spacing over the domain.

We now consider generalization to different grid resolutions, which results in a distribution shift between testing and training data. Refining the grid spacing assigns fewer eddies to the subfilter scales but more eddies to the resolved scales, leading to weaker subfilter fluxes but stronger velocity gradients. Figure 1(c) shows snapshots of ANN predictions at a grid resolution which is finer (0.4°) compared to that used for training (0.9°). The baseline ANN parameterization (Eq. (9)) predicts subfilter fluxes at a new grid resolution with a reasonably high pattern correlation (0.75). However, the magnitude of the prediction is too large, resulting in a low $\mathrm{R}^2$ ($-6.16$). Instead, the ANN with dimensional scaling (Eq. (11)) naturally accounts for the reduction of the grid spacing and reduces the magnitude of the prediction, resulting in high pattern correlation (0.92) and $\mathrm{R}^2$ (0.83) metrics (Figure 1(c)).

The generalization to both finer and coarser grids, and additionally to different depths, is summarized in Figure 1(d). At coarser grid spacings (1.2°, 1.5°) compared to that used for training (0.9°), the local dimensional scaling again helps to achieve higher $\mathrm{R}^2$ by increasing the magnitude of the prediction. In the deep layers, the subfilter fluxes and velocity gradients are considerably smaller than near the surface. Thus, a baseline ANN, trained near the surface (such as here, at depth 5m), can lead to overestimating the magnitude of the prediction at depth, resulting in a negative $\mathrm{R}^2$. However, the local dimensional scaling adjusts the prediction proportionally to the square magnitude of the velocity gradients. It improves the generalization to deep unseen layers, resulting in a high $\mathrm{R}^2$ ($\approx 0.8$ at resolution 0.9°).

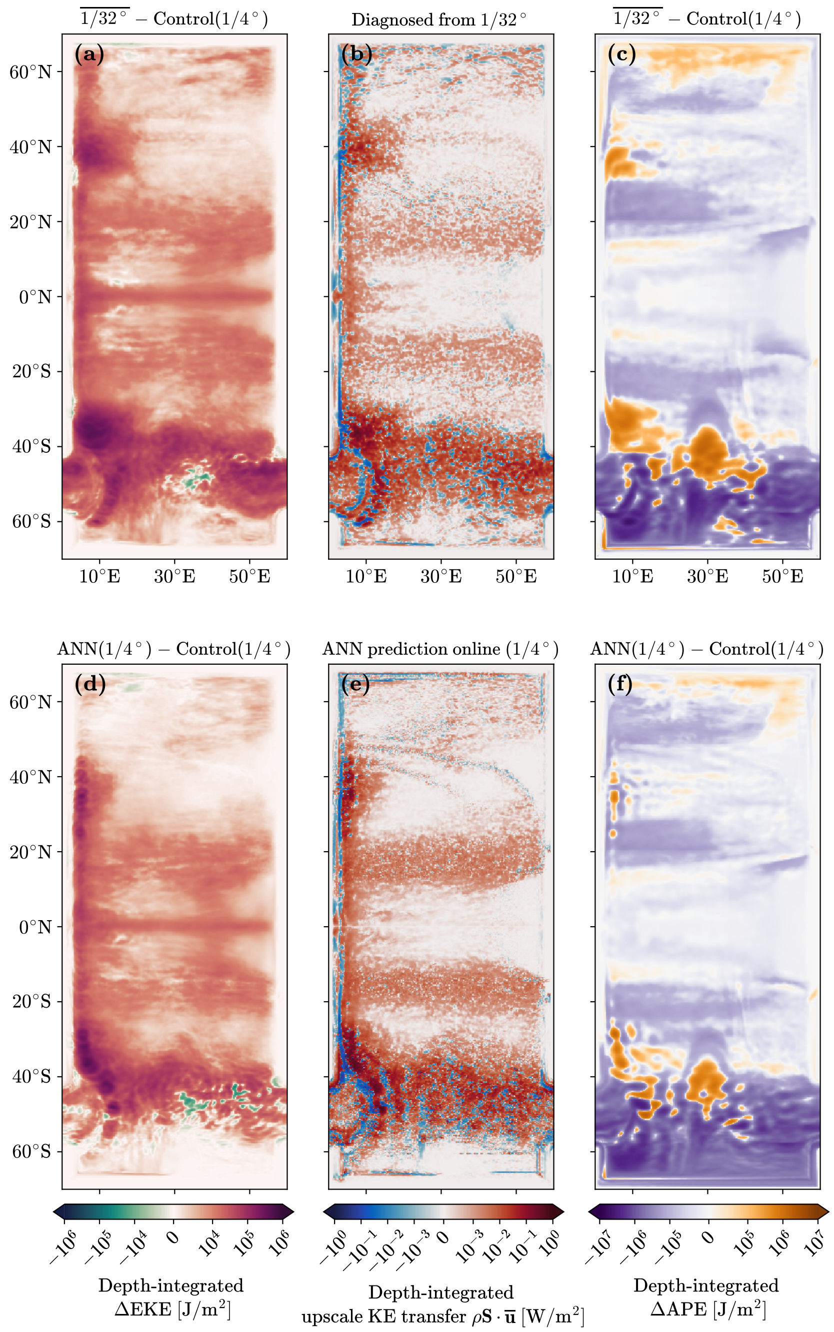


**Figure 2.** Effect of increasing resolution in idealized configuration NeverWorld2 (Marques et al., 2022) in the upper row, where $\overline{1/32°}$ represents filtered and coarse-grained high-resolution simulation. Impact of the ANN parameterization with local dimensional scaling (Eq. (11)) online at resolution $1/4°$ in the lower row. We consider three depth-integrated metrics: difference (denoted as $\Delta$) in Eddy Kinetic Energy (EKE) (left column); diagnosed and predicted online upscale kinetic energy transfer (center column) (positive values represent backscatter); difference in Available Potential Energy (APE) (right column). All metrics are averaged over 160 snapshots corresponding to the last 800 days of the simulations.

### 4.2 Online evaluation in the MOM6 ocean model

We implement the proposed mesoscale eddy parameterization and evaluate it online in two considerably different configurations of the GFDL MOM6 ocean model (Adcroft et al., 2019). The difference between the two different ocean configurations and the training set (CM2.6) in horizontal resolution, vertical coordinate, numerics, and topography motivated us to use all depths and grid resolutions shown in Figure 1(d) for training. The retrained ANN with the local dimensional scaling (Eq. (11)) has a comparable offline skill to the version described earlier, but is less tied to any specific resolution or depth. The ANN parameterization, as expected, occasionally predicts upgradient fluxes, which can cause numerical instabilities. Therefore, the grid-scale dissipation is used and given by a biharmonic Smagorinsky scheme with viscosity coefficient $\nu_4 = 0.06\sqrt{\overline{\sigma}_S^2 + \overline{\sigma}_T^2}\Delta^4$ (Adcroft et al., 2019), applied in control and parameterized (mixed modeling, Meneveau and Katz (2000)) simulations. Note that we aimed to implement the ANN parameterization without any modifications. However, some adjustments were necessary for numerical stability in an idealized ocean configuration, see implementation details in Text S3 in SI.

#### *4.2.1 Idealized configuration NeverWorld2*

We first consider an idealized adiabatic ocean configuration NeverWorld2 (NW2, Marques et al. (2022)), which generates various circulation patterns similar to the global ocean but allows us to isolate the effect of mesoscale eddies. Our goal is to show that the impact of the ANN parameterization on the flow is similar to that of increasing the horizontal resolution.

The NW2 configuration is based on the stacked shallow water equations with 15 fluid layers. The configuration includes an idealized Southern Ocean with a reentrant channel and an idealized Mid-Atlantic Ridge spanning both hemispheres. The circulation is driven by a steady wind forcing and consists of an idealized Antarctic Circumpolar Current (ACC), and Gyres circulation. We initialize coarse simulations at rest, and run for 30000 days, similar to Marques et al. (2022) and Perezhogin, Zhang, et al. (2024).

Mesoscale eddies extract available potential energy (APE) from the mean flow, which is then converted into the eddy kinetic energy (EKE) (Salmon, 1980). At an eddy-permitting resolution (1/4°), this energy pathway is partially unresolved (Jansen & Held, 2014; Mana & Zanna, 2014; Juricke et al., 2019; Loose, Bachman, et al., 2023). As a result, the coarse ocean model has too low EKE and too large APE when compared to the filtered and coarse-grained high-resolution simulation, denoted as $\overline{1/32^\circ}$ (Figure 2(a,c)). However, Figure 2(a) suggests that the missing eddies can be nominally resolved on the coarse grid. Traditional backscatter parameterizations are designed to directly reduce this EKE bias by energizing the resolved eddies (Jansen & Held, 2014). More energetic eddies extract more APE via enhanced turbulent mixing (Yankovsky et al., 2024).

Eddy backscatter is diagnosed when the kinetic energy transfer produced by the subfilter forcing (Eq. (3)) is predominantly positive (upscale), as shown in Figure 2(b). We verified that our ANN parameterization accurately predicts the eddy backscatter offline (Figure S1 in SI), suggesting reasonable generalization capabilities of our approach. In Figure 2(e), we show a more challenging task – the prediction of the eddy backscatter online once the ANN is coupled to the coarse ocean model. The online prediction of eddy backscatter grossly resembles the diagnosed data shown in Figure 2(b), although there are slight differences caused by the difference in distributions of input features.

The kinetic energy injection from the ANN parameterization leads to an increase in EKE that aligns with the high-resolution data, in particular in the ACC region (40°S−60°S), near the western boundaries, and in the subtropics (20°S−20°N), see Figure 2(d). However, the EKE increase in western boundary current extension (40°N, 10°E−20°E) and subpolar gyre (50°N−70°N) is smaller than expected from the high-resolution simulation. The spatial pattern of APE reduction in the parameterized simulation is close to that produced by increasing horizontal resolution (Figure 2(f)). The APE is predominantly reduced in the Southern Ocean and ACC regions (40°S−70°S), followed by APE reduction in gyres (20°N − 60°N, 20°S − 40°S). Local patches of APE increase in the higher resolution model (Figure 2(c)) correspond to enhanced horizontal recirculation and are reproduced by the ANN parameterization, but less accurately compared to the diagnosed APE reduction.

#### *4.2.2 Global ocean-sea-ice model OM4*

We next evaluate the ANN parameterization in the global ocean model OM4 (Adcroft et al., 2019). Unlike in the idealized configuration, the interaction of many physical processes in driving the circulation in the global ocean model impede our ability to directly isolate the effect of mesoscale eddies (Ferrari & Wunsch, 2009; Lévy et al., 2010). Building on the dynamical expectations established in the idealized NW2 configuration, our goal is to assess whether the global ocean model exhibits similar response patterns to the eddy parameterization.

The OM4 configuration is a coupled ocean-sea-ice model forced on the air-sea interface by prescribing the atmosphere state according to the CORE-II interannual forcing (IAF) protocol (Large & Yeager, 2009). The simulations span 60 years (1948-2007) and were initialized with a state of the Control model at year 1977 (after 270 years of spin-up following the repeating CORE-II IAF protocol).

The prediction of the kinetic energy injection by the ANN parameterization online is shown in Figure 3(a). Similarly to the idealized configuration, the kinetic energy is injected in the subtropical gyres, near the western boundaries, and occasionally in the ACC region. The energy injection is accompanied by an increase of the EKE in the same locations, see Figure 3(b). However, compared to the pattern found in an idealized configuration, the EKE decrease appears more frequently: along topographic features in the subpolar gyres of the North Atlantic and North Pacific oceans, and occasionally in the ACC region. The decrease of EKE in these regions is due to a shift or weakening of the mean currents, potentially as a result of the removal of kinetic energy by the ANN parameterization along the lateral boundaries, changes in deep water formation, and/or changes in global overturning circulation. The complexity of the model prohibits us from identifying a single mechanism.

Similarly to the idealized configuration, APE is primarily reduced in the Southern Ocean, with minor APE reductions observed in the Subpolar Gyres of the North Atlantic and North Pacific oceans. APE is additionally reduced in the Arctic Ocean despite the lack of eddy activity in this region. However, this reduction likely represents a change in the global reference density profile used to compute the APE.

## 5 Discussion

We discuss the implications of our results, highlighting a few lessons learned.

**Role of the grid spacing in the prediction.** Here we consider the alternatives to the local dimensional scaling (Eq. (11)) which invokes the coarse grid spacing as a length scale. Instead of using grid spacing that way, we tried to pass it as an input feature (Eq. (10)). This approach gives comparable offline performance for multiple coarse resolutions as long as they are included in the training dataset. In contrast, improving the prediction in the full water column does not require additional inputs – this can be achieved by including multiple depths into the training dataset and increasing the neural network size. These results further support our claim in Section 2.2 that efficient normalization

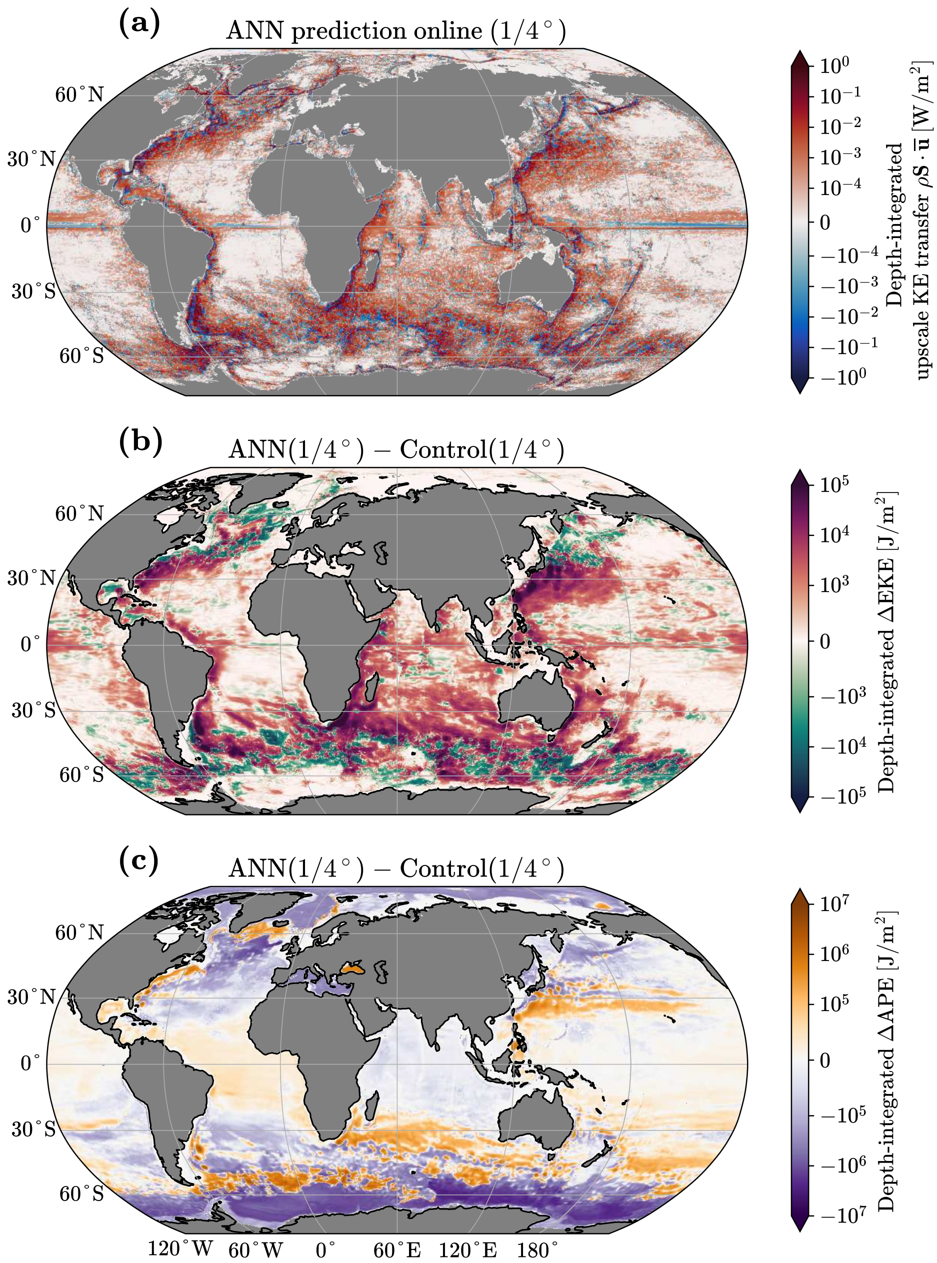


**Figure 3.** Online evaluation of the ANN parameterization in the global ocean-ice model OM4 (Adcroft et al., 2019) at eddy-permitting resolution (1/4°). The following depth-integrated diagnostics are averaged over a year of 2003: (a) upscale kinetic energy transfer predicted by the ANN parameterization online, (b) difference in Eddy kinetic energy (EKE), (c) difference in Available potential energy (APE).

starts with identifying which dimensional features are essential for accurate prediction. Incorporating local dimensional scaling as done in this work, therefore, requires less training data and smaller networks to achieve similar skill on in-distribution data, while also improving generalization to unseen grid spacings and depths.

**Implications of APE changes in NW2.** The accurate representation of APE considered in this study directly impacts metrics relevant to the global ocean. The reduction in APE leads to flattening of isopycnals and improves the structure of isopycnal interfaces across multiple cross-sections in NW2 (Figure S3 in SI), along with a weakening of ACC transport through the Drake Passage (Table S3 in SI).

**Parameterization at coarser and finer resolutions.** We performed online simulations at resolutions 1/3°, 1/4°, and 1/6° in NW2 with the ANN parameterization and existing backscatter schemes (Yankovsky et al., 2024; Perezhogin, Zhang, et al., 2024). Across these resolutions, the ANN parameterization performs similarly or better than the baselines in representing the structure of isopycnal interfaces, with more accurate results found at finer resolutions (1/4°, 1/6°), see Table S2 in SI. Implementation of the ANN parameterization at 1/2° resolution did not lead to any robust improvements compared to the control simulation. At this resolution in NW2, we are faced with less resolved eddies, weaker velocity gradients, and stronger eddy viscosity. All of these changes might contribute to the poor performance of the parametrization at this resolution. At coarser resolutions ($\approx 1°$), offline learning of the subfilter fluxes is even more challenging as the Rossby deformation radius is no longer resolved (Figure S2 in SI). At this resolution, bulk approaches for parameterizations might be more reliable. In addition, the extraction of available potential energy might also be more important to directly parameterize (Bachman, 2019; Jansen et al., 2019; Grooms et al., 2024; Perezhogin, Balakrishna, & Agrawal, 2024).

**Global ocean model biases.**

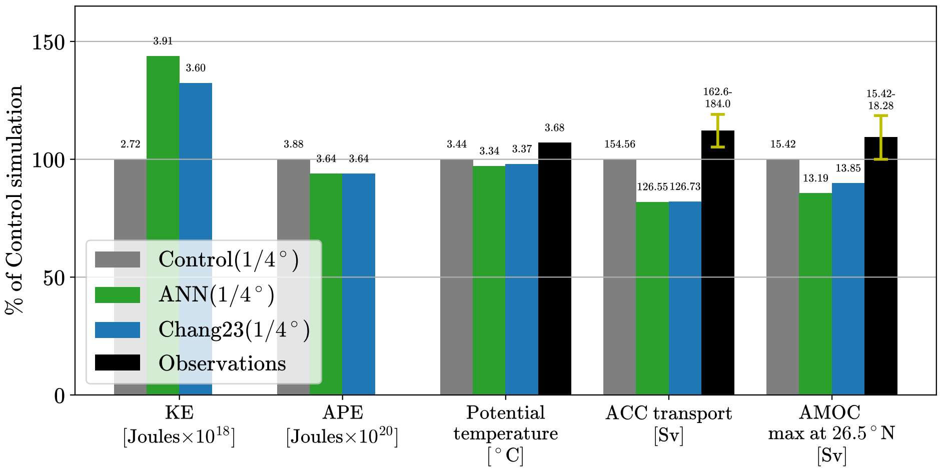


**Figure 4.** Comparison of the ANN parameterization to the negative viscosity backscatter parameterization (Chang et al., 2023) in the global ocean-ice model OM4. Kinetic energy (KE) and Available potential energy (APE) are integrated globally. Potential temperature is averaged globally. ACC transport is computed at the Drake Passage section at 70°W, and AMOC is computed as the maximum over depth streamfunction at 26.5°N. Model output is averaged over the years 1981-2007. Observational data for potential temperature is given by World Ocean Atlas 2018 (WOA18, Locarnini et al. (2018)), for ACC transport with error bar is given by cDrake (Donohue et al., 2016), and for AMOC is given by RAPID (Cunningham et al., 2007) averaged over 2004-2021 years with error bar showing interannual standard deviation.

We examined responses in more complex metrics of the global ocean circulation as opposed to APE/KE. For this purpose, we confront our ANN parameterization to a traditional anti-viscosity parameterization representing mesoscale eddy effects (Jansen et al., 2015) and already tested in OM4 by Chang et al. (2023).

Following the analysis of Chang et al. (2023), we found that both ANN and anti-viscosity parameterizations reduce the regional biases in the Gulf Stream region, see Figure S4 in SI for the biases in sea surface temperature and salinity. The response in other metrics of the global ocean circulation is remarkably similar for both parameterization approaches as well, see Figure 4. Specifically, both parameterizations increase the globally integrated kinetic energy by roughly the same percentage and reduce the APE by nearly the same percentage. The restratification effect of mesoscale eddies leads to the reduction of the globally-averaged potential temperature (Griffies et al., 2015; Adcroft et al., 2019). As discussed before, the transport through the Drake Passage is reduced in both simulations with the anti-viscosity and ANN parameterizations, see also Grooms et al. (2024). Unlike in Chang et al. (2023), both parameterizations weaken the Atlantic meridional circulation (AMOC). This suggests that the AMOC response depends on the ocean model state, perhaps to a greater extent than the details of mesoscale eddy parameterizations. The response of some global metrics (ACC, AMOC, globally-averaged potential temperature) does not project onto the existing ocean model biases. That is, both parameterized ocean simulations are less consistent with the observational data (Figure 4). Here, we note that the goal was to test the effect of the parameterizations, rather than reducing model biases. In particular, a full recalibration of the ocean model might be needed, particularly for physical processes that compete with mesoscale eddies in setting ACC and AMOC strength and average potential temperature.

## 6 Conclusions

We address the generalization issue of ANN parameterizations of mesoscale eddies by embedding physical constraints into the inputs, outputs, and parametrization itself. The Buckingham (1914)'s Pi-theorem and dimensional analysis are invoked to obtain local normalization coefficients. The ANN parameterization with local dimensional scaling significantly outperforms the ANN with fixed normalization coefficients offline, demonstrating superior generalization to unseen grid resolutions and depths in the global ocean data CM2.6. A general algorithm for constructing dimensional scaling is discussed, which can be applied to other neural-network parameterizations.

The proposed ANN parameterization with dimensional scaling is successfully tested online in the GFDL MOM6 ocean model. It accurately predicts upscale kinetic energy transfer, despite many challenges presented by online implementation. The parameterization modifies the energy pathways by energizing the resolved eddies and reducing APE, consistent with the expected restratification effects of mesoscale eddies. These improvements hold across idealized (NW2) and global ocean (OM4) configurations, with the most pronounced APE reduction occurring in the Southern Ocean. The ANN parameterization generalizes well in diverse online simulations. Specifically, the ANN achieves comparable or better online results than existing backscatter parameterizations (Chang et al., 2023; Yankovsky et al., 2024; Perezhogin, Zhang, et al., 2024), without requiring significant retuning between idealized and global ocean configurations. Moreover, the ANN performs well online in NW2 for a range of eddy-permitting resolutions ($1/3°$, $1/4°$, $1/6°$) without retuning. However, generalization to very coarse resolutions ($1°-1/2°$) requires further research as the deformation radius is not resolved and other eddy effects might need to be captured. Additional work is needed to enhance data-driven parameterizations beyond the performance of traditional parameterizations in realistic setups such as the global ocean. Both parameterization approaches exhibit substantial departures from observations and contribute comparably to persistent model biases. This highlights the considerable potential for improving parameterization schemes, evaluation metrics, and model calibration in ocean modeling. Looking ahead, the generalization issue addressed in this study has immediate implications for climate models, where parameterizations must remain reliable under changing conditions.

## Open Research Section

The training algorithm, plots, ANN weights, implemented parameterization and MOM6 setups are available at `https://github.com/m2lines/ANN-momentum-mesoscale` (archived at `https://doi.org/10.5281/zenodo.15361840`). The training dataset, offline skill, and simulation data are available at `https://doi.org/10.5281/zenodo.15361379`. For high-resolution NW2 simulation data, see `https://doi.org/10.26024/f130-ev71`. Observational products can be found: WOA18 (`https://www.ncei.noaa.gov/data/oceans/woa/WOA18`) and RAPID (`https://rapid.ac.uk/data/data-download`).

**Acknowledgments**
This project is supported by Schmidt Sciences, LLC. This research was also supported in part through the NYU IT High Performance Computing resources, services, and staff expertise. This research used resources of the National Energy Research Scientific Computing Center, a DOE Office of Science User Facility supported by the Office of Science of the U.S. Department of Energy under Contract No. DE-AC02-05CH11231 using NERSC award BER-ERCAP0032655. The authors would like to thank the M$^2$LInES team, in particular, Dhruv Balwada, Alex Connolly and Nora Loose, and also Wenda Zhang and Aviral Prakash for helpful comments and discussion.

## References

Adcroft, A., Anderson, W., Balaji, V., Blanton, C., Bushuk, M., Dufour, C. O., ... others (2019). The GFDL global ocean and sea ice model OM4.0: Model description and simulation features. *Journal of Advances in Modeling Earth Systems*, *11*(10), 3167–3211. doi: https://doi.org/10.1029/2019MS001726

Bachman, S. D. (2019). The GM + E closure: A framework for coupling backscatter with the Gent and McWilliams parameterization. *Ocean Modelling*, *136*, 85–106. doi: https://doi.org/10.1016/j.ocemod.2019.02.006

Bachman, S. D., Fox-Kemper, B., & Pearson, B. (2017). A scale-aware subgrid model for quasi-geostrophic turbulence. *Journal of Geophysical Research: Oceans*, *122*(2), 1529–1554. doi: https://doi.org/10.1002/2016JC012265

Barenblatt, G. I. (1996). *Scaling, self-similarity, and intermediate asymptotics: dimensional analysis and intermediate asymptotics* (No. 14). Cambridge University Press.

Beucler, T., Gentine, P., Yuval, J., Gupta, A., Peng, L., Lin, J., ... others (2024). Climate-invariant machine learning. *Science Advances*, *10*(6), eadj7250. doi: https://doi.org/10.1126/sciadv.adj7250

Bishop, C. M., & Nasrabadi, N. M. (2006). *Pattern recognition and machine learning* (Vol. 4) (No. 4). Springer.

Bolton, T., & Zanna, L. (2019). Applications of Deep Learning to Ocean Data Inference and Subgrid Parameterization. *Journal of Advances in Modeling Earth Systems*, *11*(1), 376–399. doi: https://doi.org/10.1029/2018MS001472

Bridgman, P. W. (1922). *Dimensional analysis*. Yale university press.

Buckingham, E. (1914). On physically similar systems; illustrations of the use of dimensional equations. *Physical review*, *4*(4), 345. doi: https://doi.org/10.1103/PhysRev.4.345

Chang, C.-Y., Adcroft, A., Zanna, L., Hallberg, R., & Griffies, S. M. (2023). Remote versus local impacts of energy backscatter on the North Atlantic SST biases in a global ocean model. *Geophysical Research Letters*, *50*(21), e2023GL105757. doi: https://doi.org/10.1029/2023GL105757

Christensen, H., & Zanna, L. (2022). Parametrization in Weather and Climate Models. Oxford University Press. doi: https://doi.org/10.1093/acrefore/9780190228620.013.826

Christopoulos, C., Lopez-Gomez, I., Beucler, T., Cohen, Y., Kawczynski, C., Dunbar, O. R., & Schneider, T. (2024). Online learning of entrainment closures in a hybrid machine learning parameterization. *Journal of Advances in Modeling Earth Systems*, *16*(11), e2024MS004485. doi: https://doi.org/10.1029/2024MS004485

Connolly, A., Cheng, Y., Walters, R., Wang, R., Yu, R., & Gentine, P. (2025). Deep learning turbulence closures generalize best with physics-based methods. *Authorea Preprints*. doi: https://doi.org/10.22541/essoar.173869578.80400701/v1

Cunningham, S. A., Kanzow, T., Rayner, D., Baringer, M. O., Johns, W. E., Marotzke, J., ... others (2007). Temporal variability of the Atlantic meridional overturning circulation at 26.5 N. *science*, *317*(5840), 935–938. doi: https://doi.org/10.1126/science.1141304

Donohue, K. A., Tracey, K., Watts, D. R., Chidichimo, M. P., & Chereskin, T. (2016). Mean Antarctic Circumpolar Current transport measured in Drake Passage. *Geophysical Research Letters*, *43*(22), 11–760. doi: https://doi.org/10.1002/2016GL070319

Ferrari, R., & Wunsch, C. (2009). Ocean circulation kinetic energy: Reservoirs, sources, and sinks. *Annual Review of Fluid Mechanics*, *41*, 253–282. doi: https://doi.org/10.1146/annurev.fluid.40.111406.102139

Fox-Kemper, B., Adcroft, A., Böning, C. W., Chassignet, E. P., Curchitser, E., Danabasoglu, G., ... others (2019). Challenges and prospects in ocean circulation models. *Frontiers in Marine Science*, *6*, 65. doi: https://doi.org/10.3389/fmars.2019.00065

Griffies, S. M. (2018). *Fundamentals of ocean climate models.* Princeton University press. doi: https://doi.org/10.2307/j.ctv301gzg

Griffies, S. M., Winton, M., Anderson, W. G., Benson, R., Delworth, T. L., Dufour, C. O., ... others (2015). Impacts on ocean heat from transient mesoscale eddies in a hierarchy of climate models. *Journal of Climate*, *28*(3), 952–977. doi: https://doi.org/10.1175/JCLI-D-14-00353.1

Grooms, I., Agarwal, N., Marques, G. M., Pegion, P., & Yassin, H. (2024). The Stochastic GM+ E closure: A framework for coupling stochastic backscatter with the Gent and McWilliams parameterization. *Authorea Preprints*. doi: https://doi.org/10.22541/essoar.172118408.85625257/v1

Grooms, I., Loose, N., Abernathey, R., Steinberg, J., Bachman, S. D., Marques, G. M., ... Yankovsky, E. (2021). Diffusion-based smoothers for spatial filtering of gridded geophysical data. *Journal of Advances in Modeling Earth Systems*, *13*(9), e2021MS002552. doi: https://doi.org/10.1029/2021MS002552

Guan, Y., Subel, A., Chattopadhyay, A., & Hassanzadeh, P. (2022). Learning physics-constrained subgrid-scale closures in the small-data regime for stable and accurate LES. *Physica D: Nonlinear Phenomena*, 133568. doi: https://doi.org/10.1016/j.physd.2022.133568

Guillaumin, A. P., & Zanna, L. (2021). Stochastic-deep learning parameterization of ocean momentum forcing. *Journal of Advances in Modeling Earth Systems*, *13*(9), e2021MS002534. doi: https://doi.org/10.1029/2021MS002534

Gultekin, C., Subel, A., Zhang, C., Leibovich, M., Perezhogin, P., Adcroft, A., ... Zanna, L. (2024). An analysis of deep learning parameterizations for ocean subgrid eddy forcing. *arXiv preprint arXiv:2411.06604*. doi: https://doi.org/10.48550/arXiv.2411.06604

Hastie, T., Tibshirani, R., Friedman, J. H., & Friedman, J. H. (2009). *The elements of statistical learning: data mining, inference, and prediction* (Vol. 2). Springer.

Hewitt, H. T., Roberts, M., Mathiot, P., Biastoch, A., Blockley, E., Chassignet, E. P., … others (2020). Resolving and parameterising the ocean mesoscale in earth system models. *Current Climate Change Reports*, *6*(4), 137–152. doi: https://doi.org/10.1007/s40641-020-00164-w

Jansen, M. F., Adcroft, A., Khani, S., & Kong, H. (2019). Toward an energetically consistent, resolution aware parameterization of ocean mesoscale eddies. *Journal of Advances in Modeling Earth Systems*, *11*(8), 2844–2860. doi: https://doi.org/10.1029/2019MS001750

Jansen, M. F., & Held, I. M. (2014). Parameterizing subgrid-scale eddy effects using energetically consistent backscatter. *Ocean Modelling*, *80*, 36–48. doi: https://doi.org/10.1016/j.ocemod.2014.06.002

Jansen, M. F., Held, I. M., Adcroft, A., & Hallberg, R. (2015). Energy budget-based backscatter in an eddy permitting primitive equation model. *Ocean Modelling*, *94*, 15–26. doi: https://doi.org/10.1016/j.ocemod.2015.07.015

Juricke, S., Danilov, S., Kutsenko, A., & Oliver, M. (2019). Ocean kinetic energy backscatter parametrizations on unstructured grids: Impact on mesoscale turbulence in a channel. *Ocean Modelling*, *138*, 51–67. doi: https://doi.org/10.1016/j.ocemod.2019.03.009

Kang, M., Jeon, Y., & You, D. (2023). Neural-network-based mixed subgrid-scale model for turbulent flow. *Journal of Fluid Mechanics*, *962*, A38. doi: https://doi.org/10.1017/jfm.2023.260

Kashinath, K., Mustafa, M., Albert, A., Wu, J., Jiang, C., Esmaeilzadeh, S., … others (2021). Physics-informed machine learning: case studies for weather and climate modelling. *Philosophical Transactions of the Royal Society A*, *379*(2194), 20200093. doi: https://doi.org/10.1098/rsta.2020.0093

Large, W., & Yeager, S. (2009). The global climatology of an interannually varying air–sea flux data set. *Climate dynamics*, *33*, 341–364. doi: https://doi.org/10.1007/s00382-008-0441-3

Leith, C. (1996). Stochastic models of chaotic systems. *Physica D: Nonlinear Phenomena*, *98*(2-4), 481–491. doi: https://doi.org/10.1016/0167-2789(96)00107-8

Lévy, M., Klein, P., Tréguier, A.-M., Iovino, D., Madec, G., Masson, S., & Takahashi, K. (2010). Modifications of gyre circulation by sub-mesoscale physics. *Ocean Modelling*, *34*(1-2), 1–15. doi: https://doi.org/10.1016/j.ocemod.2010.04.001

Li, H., Xie, J., Zhang, C., Zhang, Y., & Zhao, Y. (2025). A transformer-based convolutional method to model inverse cascade in forced two-dimensional turbulence. *Journal of Computational Physics*, *520*, 113475. doi: https://doi.org/10.1016/j.jcp.2024.113475

Ling, J., Kurzawski, A., & Templeton, J. (2016). Reynolds averaged turbulence modelling using deep neural networks with embedded invariance. *Journal of Fluid Mechanics*, *807*, 155–166. doi: https://doi.org/10.1017/jfm.2016.615

Locarnini, M., Mishonov, A., Baranova, O., Boyer, T., Zweng, M., Garcia, H., … others (2018). World ocean atlas 2018, volume 1: Temperature.

Loose, N., Bachman, S., Grooms, I., & Jansen, M. (2023). Diagnosing scale-dependent energy cycles in a high-resolution isopycnal ocean model. *Journal of Physical Oceanography*, *53*(1), 157–176. doi: https://doi.org/10.1175/JPO-D-22-0083.1

Loose, N., Marques, G. M., Adcroft, A., Bachman, S., Griffies, S. M., Grooms, I., … Jansen, M. F. (2023). Comparing two parameterizations for the restratification effect of mesoscale eddies in an isopycnal ocean model. *Journal of Advances in Modeling Earth Systems*, *15*(12), e2022MS003518. doi: https://doi.org/10.1029/2022MS003518

Lund, T. S., & Novikov, E. (1993). Parameterization of subgrid-scale stress by the velocity gradient tensor. *Annual Research Briefs, 1992*.

Maddison, J. R. (2024). Online learning in idealized ocean gyres. *arXiv preprint arXiv:2412.06393*. doi: https://doi.org/10.48550/arXiv.2412.06393

Mana, P. P., & Zanna, L. (2014). Toward a stochastic parameterization of ocean mesoscale eddies. *Ocean Modelling*, *79*, 1–20. doi: https://doi.org/10.1016/j.ocemod.2014.04.002

Marques, G. M., Loose, N., Yankovsky, E., Steinberg, J. M., Chang, C.-Y., Bhamidipati, N., ... others (2022). NeverWorld2: An idealized model hierarchy to investigate ocean mesoscale eddies across resolutions. *Geoscientific Model Development*, *15*(17), 6567–6579. doi: https://doi.org/10.5194/gmd-15-6567-2022

Maulik, R., & San, O. (2017). A neural network approach for the blind deconvolution of turbulent flows. *Journal of Fluid Mechanics*, *831*, 151–181. doi: https://doi.org/10.1017/jfm.2017.637

Maulik, R., San, O., Rasheed, A., & Vedula, P. (2019). Subgrid modelling for two-dimensional turbulence using neural networks. *Journal of Fluid Mechanics*, *858*, 122–144. doi: https://doi.org/10.1017/jfm.2018.770

Meneveau, C., & Katz, J. (2000). Scale-invariance and turbulence models for large-eddy simulation. *Annual Review of Fluid Mechanics*, *32*(1), 1–32. doi: https://doi.org/10.1146/annurev.fluid.32.1.1

Pawar, S., San, O., Rasheed, A., & Vedula, P. (2020). A priori analysis on deep learning of subgrid-scale parameterizations for kraichnan turbulence. *Theoretical and Computational Fluid Dynamics*, *34*(4), 429–455. doi: https://doi.org/10.1007/s00162-019-00512-z

Perezhogin, P., Balakrishna, A., & Agrawal, R. (2024). Large eddy simulation of ocean mesoscale eddies. In *Proceedings of the Summer Program 2024, Center for Turbulence Research, Stanford University* (p. 507-516). Retrieved from `https://arxiv.org/abs/2501.05357`

Perezhogin, P., Zhang, C., Adcroft, A., Fernandez-Granda, C., & Zanna, L. (2024). A stable implementation of a data-driven scale-aware mesoscale parameterization. *Journal of Advances in Modeling Earth Systems*, *16*(10), e2023MS004104. doi: https://doi.org/10.1029/2023MS004104

Pope, S. B. (1975). A more general effective-viscosity hypothesis. *Journal of Fluid Mechanics*, *72*(2), 331–340. doi: https://doi.org/10.1017/S0022112075003382

Prakash, A., Jansen, K. E., & Evans, J. A. (2022). Invariant data-driven subgrid stress modeling in the strain-rate eigenframe for large eddy simulation. *Computer Methods in Applied Mechanics and Engineering*, *399*, 115457. doi: https://doi.org/10.1016/j.cma.2022.115457

Prakash, A., Jansen, K. E., & Evans, J. A. (2024). Invariant data-driven subgrid stress modeling on anisotropic grids for large eddy simulation. *Computer Methods in Applied Mechanics and Engineering*, *422*, 116807. doi: https://doi.org/10.1016/j.cma.2024.116807

Reissmann, M., Hasslberger, J., Sandberg, R. D., & Klein, M. (2021). Application of gene expression programming to a-posteriori les modeling of a taylor green vortex. *Journal of Computational Physics*, *424*, 109859. doi: https://doi.org/10.1016/j.jcp.2020.109859

Ross, A., Li, Z., Perezhogin, P., Fernandez-Granda, C., & Zanna, L. (2023). Benchmarking of machine learning ocean subgrid parameterizations in an idealized model. *Journal of Advances in Modeling Earth Systems*, *15*(1), e2022MS003258. doi: https://doi.org/10.1029/2022MS003258

Salmon, R. (1980). Baroclinic instability and geostrophic turbulence. *Geophysical & Astrophysical Fluid Dynamics*, *15*(1), 167–211. doi: https://doi.org/10.1080/03091928008241178

Sane, A., Reichl, B. G., Adcroft, A., & Zanna, L. (2023). Parameterizing vertical mixing coefficients in the ocean surface boundary layer using neural networks. *Journal of Advances in Modeling Earth Systems*, *15*(10), e2023MS003890. doi: https://doi.org/10.1029/2023MS003890

Schneider, T., Leung, L. R., & Wills, R. C. (2024). Opinion: Optimizing climate models with process knowledge, resolution, and artificial intelligence. *Atmospheric Chemistry and Physics*, *24*(12), 7041–7062. doi: https://doi.org/10.5194/acp-24-7041-2024

Smagorinsky, J. (1963). General circulation experiments with the primitive equations: I. the basic experiment. *Monthly weather review*, *91*(3), 99–164. doi: https://doi.org/10.1175/1520-0493(1963)091%3C0099:GCEWTP%3E2.3.CO;2

Srinivasan, K., Chekroun, M. D., & McWilliams, J. C. (2024). Turbulence closure with small, local neural networks: Forced two-dimensional and $\beta$-plane flows. *Journal of Advances in Modeling Earth Systems*, *16*(4), e2023MS003795. doi: https://doi.org/10.1029/2023MS003795

Wang, Y., Yuan, Z., Wang, X., & Wang, J. (2022). Constant-coefficient spatial gradient models for the sub-grid scale closure in large-eddy simulation of turbulence. *Physics of Fluids*, *34*(9). doi: https://doi.org/10.1063/5.0101356

Wang, Y., Yuan, Z., Xie, C., & Wang, J. (2021). Artificial neural network-based spatial gradient models for large-eddy simulation of turbulence. *AIP Advances*, *11*(5). doi: https://doi.org/10.1063/5.0053590

Xie, C., Wang, J., & E, W. (2020). Modeling subgrid-scale forces by spatial artificial neural networks in large eddy simulation of turbulence. *Physical Review Fluids*, *5*(5), 054606. doi: https://doi.org/10.1103/PhysRevFluids.5.054606

Yan, F. E., Mak, J., & Wang, Y. (2024). On the choice of training data for machine learning of geostrophic mesoscale turbulence. *Journal of Advances in Modeling Earth Systems*, *16*(2), e2023MS003915. doi: https://doi.org/10.1029/2023MS003915

Yankovsky, E., Bachman, S., Smith, K. S., & Zanna, L. (2024). Vertical structure and energetic constraints for a backscatter parameterization of ocean mesoscale eddies. *Journal of Advances in Modeling Earth Systems*, *16*(7), e2023MS004093. doi: https://doi.org/10.1029/2023MS004093

Zanna, L., & Bolton, T. (2020). Data-driven equation discovery of ocean mesoscale closures. *Geophysical Research Letters*, *47*(17), e2020GL088376. doi: https://doi.org/10.1029/2020GL088376

Zhang, C., Perezhogin, P., Gultekin, C., Adcroft, A., Fernandez-Granda, C., & Zanna, L. (2023). Implementation and evaluation of a machine learned mesoscale eddy parameterization into a numerical ocean circulation model. *Journal of Advances in Modeling Earth Systems*, *15*(10), e2023MS003697. doi: https://doi.org/10.1029/2023MS003697

# Supporting Information for "Generalizable neural-network parameterization of mesoscale eddies in idealized and global ocean models"

Pavel Perezhogin[1], Alistair Adcroft[3], Laure Zanna[1,2]

[1]Courant Institute of Mathematical Sciences, New York University, New York, NY, USA

[2]Center for Data Science, New York University, New York, NY, USA

[3]Program in Atmospheric and Oceanic Sciences, Princeton University, Princeton, NJ, USA

## Contents of this file

1. Text S1 to S3
2. Tables S1 to S3
3. Figures S1 to S4

## 1. Text S1. Traditional parameterizations as a special case of dimensional scaling

Here, we show that enforcing the dimensional scaling constraint on the ANN parameterization is not too restrictive and admits multiple traditional parameterizations as a special case with well-behaved functional representations (see Prakash, Jansen, and Evans (2022) for discussion). The ANN parameterization of subfilter momentum flux with dimensional scaling constraint is:

$$\widehat{\mathbf{T}}(\mathbf{X}, \Delta) = \Delta^2 ||\mathbf{X}||_2^2 \mathrm{ANN}_\theta(\mathbf{X}/||\mathbf{X}||_2) \equiv \tag{1}$$

$$\Delta^2 ||\mathbf{X}||_2^2 \begin{pmatrix} \mathrm{ANN}_\theta^{xx}(\mathbf{x}) & \mathrm{ANN}_\theta^{xy}(\mathbf{x}) \\ \mathrm{ANN}_\theta^{xy}(\mathbf{x}) & \mathrm{ANN}_\theta^{yy}(\mathbf{x}) \end{pmatrix}, \tag{2}$$

where the vector of input features is

$$\mathbf{X} = \begin{pmatrix} [\overline{\sigma}_S] \updownarrow_9 \\ [\overline{\sigma}_T] \updownarrow_9 \\ [\overline{\omega}] \updownarrow_9 \end{pmatrix} \in \mathbb{R}^{27} \tag{3}$$

and $\mathbf{x} = \mathbf{X}/||\mathbf{X}||_2$.

**Smagorinsky parameterization:** We first consider a Smagorinsky (1963) subgrid parameterization:

$$\widehat{\mathbf{T}} = C_S \Delta^2 \sqrt{\overline{\sigma}_S^2 + \overline{\sigma}_T^2} \begin{pmatrix} \overline{\sigma}_T & \overline{\sigma}_S \\ \overline{\sigma}_S & -\overline{\sigma}_T \end{pmatrix}. \tag{4}$$

This subgrid model can be given in the form of Eq. (2) if ANN parameterizes the following functions:

$$\mathrm{ANN}_\theta^{xx}(\mathbf{x}) = C_S x_{14} \sqrt{x_5^2 + x_{14}^2} \tag{5}$$

$$\mathrm{ANN}_\theta^{yy}(\mathbf{x}) = -\mathrm{ANN}_\theta^{xx}(\mathbf{x}) \tag{6}$$

$$\mathrm{ANN}_\theta^{xy}(\mathbf{x}) = C_S x_5 \sqrt{x_5^2 + x_{14}^2}, \tag{7}$$

where $x_5$ and $x_{14}$ represent components of the non-dimensional vector $\mathbf{x}$ which are equal to $\overline{\sigma}_S/||\mathbf{X}||_2$ and $\overline{\sigma}_T/||\mathbf{X}||_2$ in the center of $3 \times 3$ spatial stencil, respectively. The derived functions are well-behaved on a bounded domain ($|x_i| \leq 1$), and thus they can be easily learned with the ANN. The functional representations of the parameterizations derived below are well-behaved as well.

**Zanna-Bolton 2020 parameterization:** Similarly, we can show that Zanna and Bolton (2020) parameterization

$$\widehat{\mathbf{T}} = -\gamma\Delta^2 \begin{pmatrix} -\overline{\omega}\,\overline{\sigma}_S & \overline{\omega}\,\overline{\sigma}_T \\ \overline{\omega}\,\overline{\sigma}_T & \overline{\omega}\,\overline{\sigma}_S \end{pmatrix} - \frac{1}{2}\gamma\Delta^2(\overline{\omega}^2 + \overline{\sigma}_T^2 + \overline{\sigma}_S^2) \begin{pmatrix} 1 & 0 \\ 0 & 1 \end{pmatrix} \tag{8}$$

can be represented as follows:

$$\mathrm{ANN}_\theta^{xx}(\mathbf{x}) = \gamma x_5 x_{23} - \frac{1}{2}\gamma(x_5^2 + x_{14}^2 + x_{23}^2), \tag{9}$$

$$\mathrm{ANN}_\theta^{yy}(\mathbf{x}) = -\gamma x_5 x_{23} - \frac{1}{2}\gamma(x_5^2 + x_{14}^2 + x_{23}^2), \tag{10}$$

$$ANN_\theta^{xy}(\mathbf{x}) = -\gamma x_{14} x_{23}. \tag{11}$$

**Leith 1996 parameterization:** Next, we consider Leith (1996) parameterization:

$$\widehat{\mathbf{T}} = C_L\Delta^3|\nabla\overline{\omega}| \begin{pmatrix} \overline{\sigma}_T & \overline{\sigma}_S \\ \overline{\sigma}_S & -\overline{\sigma}_T \end{pmatrix}. \tag{12}$$

By approximating the gradient with central differences and assuming an isotropic and uniform grid, we obtain:

$$\mathrm{ANN}_\theta^{xx}(\mathbf{x}) = \frac{1}{2} C_L x_{14} \sqrt{(x_{24} - x_{22})^2 + (x_{26} - x_{20})^2}, \tag{13}$$

$$\mathrm{ANN}_\theta^{yy}(\mathbf{x}) = -\mathrm{ANN}_\theta^{xx}(\mathbf{x}), \tag{14}$$

$$\mathrm{ANN}_\theta^{xy}(\mathbf{x}) = \frac{1}{2} C_L x_5 \sqrt{(x_{24} - x_{22})^2 + (x_{26} - x_{20})^2} \tag{15}$$

**Biharmonic Smagorinsky parameterization:** The biharmonic Smagorinsky subgrid model has the form:

$$\widehat{\mathbf{T}} = -C_S \Delta^4 \sqrt{\overline{\sigma}_S^2 + \overline{\sigma}_T^2} \nabla^2 \begin{pmatrix} \overline{\sigma}_T & \overline{\sigma}_S \\ \overline{\sigma}_S & -\overline{\sigma}_T \end{pmatrix}. \tag{16}$$

By approximating the $\nabla^2$ operator on an isotropic and uniform grid, we obtain:

$$\mathrm{ANN}_\theta^{xx}(\mathbf{x}) = -C_S (x_{15} + x_{13} + x_{17} + x_{11} - 4x_{14}) \sqrt{x_5^2 + x_{14}^2}, \tag{17}$$

$$\mathrm{ANN}_\theta^{yy}(\mathbf{x}) = -\mathrm{ANN}_\theta^{xx}(\mathbf{x}), \tag{18}$$

$$\mathrm{ANN}_\theta^{xy}(\mathbf{x}) = -C_S (x_6 + x_4 + x_8 + x_2 - 4x_5) \sqrt{x_5^2 + x_{14}^2}. \tag{19}$$

## 2. Text S2. Training dataset and training algorithm

### 2.1. Dataset

Following Guillaumin and Zanna (2021), the training dataset used is from the GFDL CM2.6 climate model (Griffies et al., 2015) with 0.1° nominal resolution for the ocean component. We produce a vast training dataset of subfilter forcing to explore generalization. Specifically, the subfilter forcing is created using four coarse-graining factors, selected to be similar to those used in Gultekin et al. (2024), and 10 depths (extending Gultekin et al. (2024)), see Table S1. The dataset consists of filtered and coarse-grained velocity gradients (Eq. (7)) and subfilter forcing (Eq. (3)).

### 2.2. Training algorithm and boundary conditions

We train the ANN model on data from the full globe, similarly to Gultekin et al. (2024). The loss function is defined to optimize for the divergence ($\nabla \cdot$ ) of subfilter fluxes ($\mathbf{T}$) similarly to Zanna and Bolton (2020) and Srinivasan, Chekroun, and McWilliams (2024). The mean squared error (MSE) loss is minimized on every 2D snapshot of subfilter forcing

$\mathbf{S}$ and normalized by the corresponding $l_2$-norm of $\mathbf{S}$ (Agdestein & Sanderse, 2025):

$$\mathcal{L}_{\mathrm{MSE}} = ||(\mathbf{S} - \nabla \cdot \widehat{\mathbf{T}}) \cdot m||_2^2 / ||\mathbf{S} \cdot m||_2^2, \tag{20}$$

where $m$ is the mask of wet points. The input features (velocity gradients, $\mathbf{X}$) and predicted subfilter fluxes are set to zero on the land as well: $\widehat{\mathbf{T}} \equiv m \cdot \widehat{\mathbf{T}}(m \cdot \mathbf{X})$. That is, we impose zero Neumann boundary condition (Zhang et al., 2024) and free-slip boundary condition. We found that including the grid points adjacent to the land to the loss function is essential for ensuring the numerical stability of online runs. Another important design choice for online numerical stability is performing the ANN inference on the collocated, rather than on the staggered grid, similarly to Guillaumin and Zanna (2021) and Agdestein and Sanderse (2025). The loss function (Eq. (20)) is evaluated and minimized for a total of 16000 two-dimensional snapshots during training, see Table S1.

### 2.3. ANN model architecture

The ANN model is chosen to be small (see Table S1): it has only a single hidden layer with 20 neurons, as in Prakash et al. (2022), with a total of 623 trainable parameters. Increasing the number of parameters 60 times reduces the MSE loss averaged over the dataset from $\mathcal{L}_{\mathrm{MSE}} \approx 0.5$ to $\mathcal{L}_{\mathrm{MSE}} \approx 0.335$. However, we keep our ANN small, within $\mathcal{O}(1000)$ parameters, to bound the ANN inference time within $\approx 10\%$ of the ocean model runtime. We verified that tripling of the number of ANN parameters has only a marginal effect on fields produced in online numerical tests. Specifically, we find little to no effect on the 5-year simulated mean fields in online global ocean model runs or the kinetic energy in a two-layer Double Gyre configuration.

### 2.4. Sensitivity to the random seed

The R-squared of the offline predictions of the ANN is almost insensitive to the random seed used to initialize the training algorithm. In addition, the prediction errors $\mathbf{S}-\nabla\cdot\widehat{\mathbf{T}}$ are highly correlated between different seeds (as in Srinivasan et al. (2024)). We also confirmed that the kinetic energy is nearly unchanged in online two-layer Double Gyre experiments, using ANNs generated from different initializations of the training algorithm, similarly to Zhang et al. (2024). However, there is some sensitivity to the training algorithm initialization for the mean flow prediction: the response pattern in the mean flow is similar, but the response magnitude can vary by 50%. The sensitivity to the random seed is not apparent in the global ocean configuration OM4.

### 2.5. Choice of the filter scale in the training dataset

We produce the training data using a Gaussian filter implemented in the package GCM-Filters (Grooms et al., 2021; Loose et al., 2022) with width $\overline{\Delta}$, chosen in relation to the coarse grid spacing $\Delta$. The filter-to-grid width ratio parameter (FGR $= \overline{\Delta}/\Delta$) represents the strength of the subfilter parameterization: relatively low value of FGR ($\overline{\Delta}/\Delta = 1$) in the training dataset results in a learned parameterization that has negligible effect in online simulations. On the other hand, a relatively large value (FGR $= 4$) results in over-energized grid-scale features. The value used here (FGR $= 3$) corresponds to the strongest parameterization effect without generating grid-scale noise. Note that the optimal FGR parameter depends on the numerical and physical dissipation schemes present in the ocean model, as the ANN subfilter parameterization alone does not produce enough grid-scale dissipation. For the discussion of how to choose FGR parameter see Perezhogin, Balakrishna, and Agrawal (2024); Perezhogin, Zhang, Adcroft, Fernandez-Granda, and Zanna (2024); Perezhogin and Glazunov (2023).

## 3. Text S3. Online implementation and numerical stability in MOM6

The trained parameters of the ANN subfilter model are saved to a NetCDF file and read by the numerical ocean model during initialization. The neural network inference is implemented using the Fortran module of Sane, Reichl, Adcroft, and Zanna (2023). The ANN inference takes $\approx 10\%$ of the ocean model runtime, for a neural network with one hidden layer and 20 neurons. However, the inference can be further accelerated, as we found that the inference in Python is generally faster than in Fortran.

The implemented ANN parameterization works stably (free of NaNs in prognostic fields) in idealized Double Gyre and global ocean OM4 configurations, without any tuning, in part because the biharmonic Smagorinsky model provides the dissipation. In the idealized configuration NeverWorld2 (NW2, Marques et al. (2022)), however, tuning is required to improve the numerical stability even when a backscatter parameterization (whether our ANN or more traditional parametrization) is used together with biharmonic Smagorinsky model; e.g., Yankovsky, Bachman, Smith, and Zanna (2024). We have modified the ANN parameterization to achieve stability, without optimizing for online metrics, using a set of minimal changes. Our tuning includes attenuating the magnitude of the ANN parameterization in high-strain regions following Perezhogin, Zhang, et al. (2024) and allowing the MOM6 dynamical core to truncate velocities if they are too big. Additionally, at resolution $1/6°$ in NW2, we had to reduce the time stepping interval.

**Table S1.** Parameters of the training data and artificial neural network (ANN) model

| Category | Value |
|---|---|
| **Training Data Parameters** | |
| High-resolution data | CM2.6 (Griffies et al., 2015), 0.1° ocean grid |
| Diagnosed features | $\overline{\sigma}_S$, $\overline{\sigma}_T$, $\overline{\omega}$, $\mathbf{S}$ |
| Layer Depths (m) | 5, 55, 110, 180, 330, 730, 1500, 2500, 3500, 4500 |
| Coarse Grid Spacing, $\Delta$ | 0.4°, 0.9°, 1.2°, 1.5° |
| Gaussian Filter Width, $\overline{\Delta}$ | 1.2°, 2.7°, 3.6°, 4.5°; i.e., $\overline{\Delta}/\Delta = 3$ |
| Training / Validation / Test Splitting (years) | $181 - 188$ / $194$ / $199 - 200$ |
| Snapshot Averaging Interval | 5 days |
| Time Seperation Between Snapshots | 1 month |
| Number of 2D Snapshots used for Training | $10 \times 4 \times 8 \times 12 = 3840$ |
| Number of Training Iterations | 16000 (each iteration randomly selects 2D snapshot) |
| **ANN Parameters** | |
| Input Size | $3 \times 3$ |
| Number of Hidden Layers | 1 |
| Number of Channels in Hidden Layer | 20 |
| Activation Function | ReLU |
| Number of Trainable Parameters | 623 |

| RMSE | 0°E | 15°E | 30°E | 45°E |
|---|---|---|---|---|
| Control(1/3°) | 51.3 | 46.8 | 49.1 | 36.8 |
| Yankovsky24(1/3°) | 33.5 | 31.6 | 29.9 | 27.4 |
| ZB20-Reynolds(1/3°) | **32.7** | 25.4 | **26.1** | **21.6** |
| ANN(1/3°) | 35.0 | **24.3** | 30.9 | 28.6 |
| Control(1/4°) | 52.1 | 42.1 | 40.3 | 34.6 |
| Yankovsky24(1/4°) | 27.8 | 23.0 | 20.7 | 21.3 |
| ZB20-Reynolds(1/4°) | **26.9** | 21.0 | 18.4 | **18.5** |
| ANN(1/4°) | 29.2 | **20.0** | **16.7** | 19.7 |
| Control(1/6°) | 42.7 | 30.7 | 31.8 | 26.7 |
| Yankovsky24(1/6°) | 26.2 | 22.3 | 16.1 | 16.8 |
| ZB20-Reynolds(1/6°) | 27.7 | 24.5 | 18.9 | 18.4 |
| ANN(1/6°) | **23.5** | **18.8** | **13.8** | **14.6** |

**Table S2.** Online results in idealized configuration NeverWorld2 at three coarse resolutions (1/3°, 1/4° and 1/6°). The root mean squared errors (RMSE) in 1000-day averaged position of interfaces over four meridional transects at longitudes 0°E, 15°E, 30°E and 45°E. RMSE units are metres. The interfaces for Control and ANN-parameterized runs at resolution 1/4° at longitudes 0°E and 45°E are also shown in Figure S3. The error is computed w.r.t. 1/32° model. Yankovsky24 stands for parameterization of Yankovsky et al. (2024), ZB20-Reynolds stands for Zanna and Bolton (2020) parameterization implemented and modified by Perezhogin, Zhang, et al. (2024). Parameterizations are not retuned when resolution is changed.

| | ACC transport [Sv] |
|---|---|
| 1/32° | 235.3 |
| Control(1/3°) | 242.7 |
| Yankovsky24(1/3°) | **237**.**4** |
| ZB20-Reynolds(1/3°) | 230.2 |
| ANN(1/3°) | 241.6 |
| Control(1/4°) | 245.1 |
| Yankovsky24(1/4°) | 229.9 |
| ZB20-Reynolds(1/4°) | 225.4 |
| ANN(1/4°) | **236**.**9** |
| Control(1/6°) | 243.3 |
| Yankovsky24(1/6°) | **230**.**4** |
| ZB20-Reynolds(1/6°) | 219.5 |
| ANN(1/4°) | 228.8 |

**Table S3.** Online results in idealized configuration NeverWorld2. The ACC transport through the Drake Passage at 0°E averaged over 800 days.

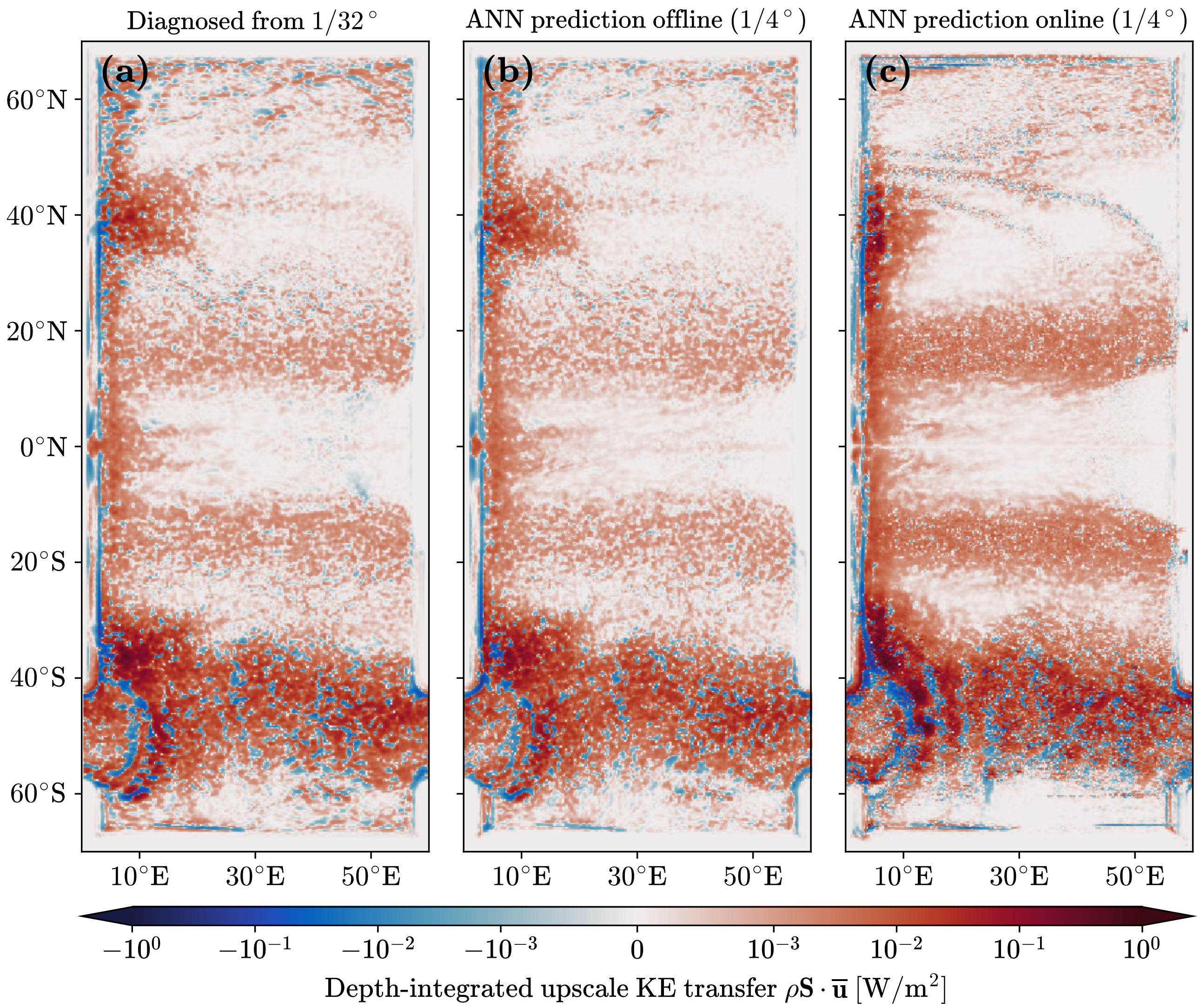


**Figure S1.** Upscale KE transfer (positive numbers correspond to backscatter) averaged over 800 days and integrated over depth in idealized NeverWorld2 configuration. (a) Diagnosed from high-resolution (1/32°) simulation by filtering and coarsegraining, (b) and (c) predicted by the ANN offline and online, respectively, at coarse resolution 1/4°. The ANN was trained on global ocean data and thus generalizes well to a new configuration as seen in the accurate prediction of KE transfer offline. Prediction offline means that filtered and coarsegrained snapshots of the high-resolution model were given as inputs to the ANN. Slight degradation of prediction online is related to the difference in magnitude of small-scale velocity gradients and large-scale circulation patterns in the coarse ocean model.

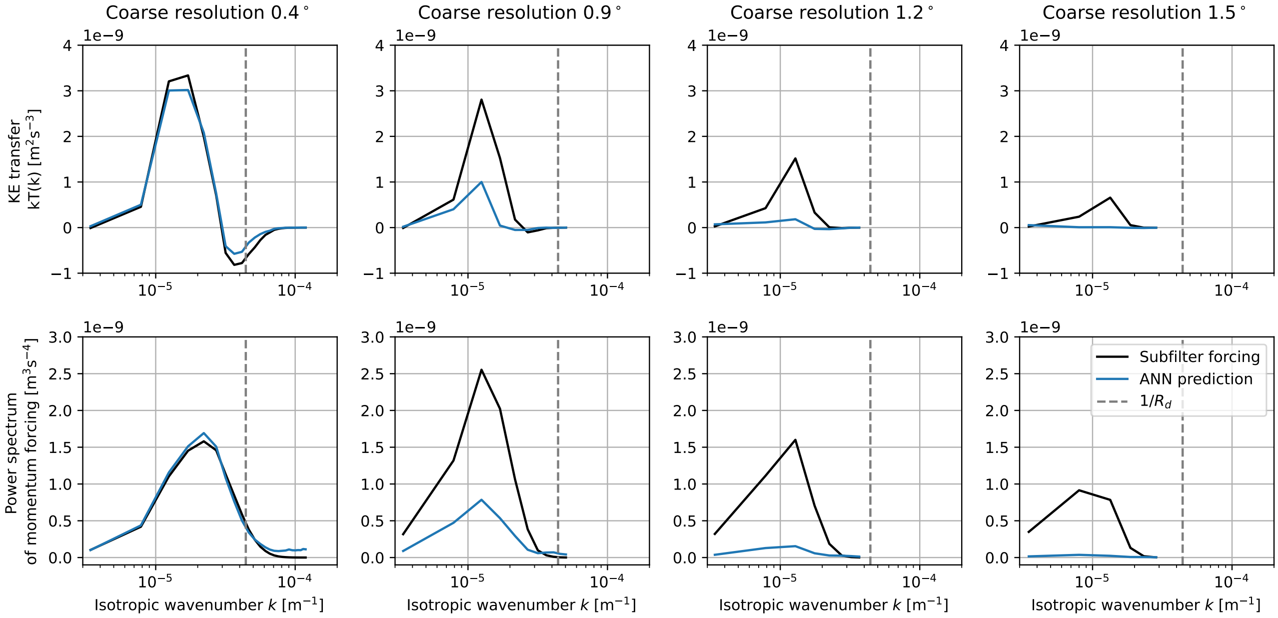


**Figure S2.** (Upper row) Offline kinetic energy (KE) transfer spectrum, where $T(k) = 2\pi k Re(\mathcal{F}(\mathbf{u})^* \mathcal{F}(\mathbf{S}))$, and $\mathcal{F}$ is the 2D Fourier transform, $Re$ is the real part, and $*$ is the complex conjugate. (Lower row) power spectrum of subfilter forcing $2\pi k \mathcal{F}(\mathbf{S})^* \mathcal{F}(\mathbf{S})$. Spectra are computed in the North Atlantic region $(25-45°\text{N}) \times (60-40°\text{W})$ and at depth 5m. $R_d = 22.6\text{km}$ is the Rossby deformation radius in this region. A single ANN is trained on all available training data. Each column shows evaluation of ANN at different resolutions of a coarse grid.

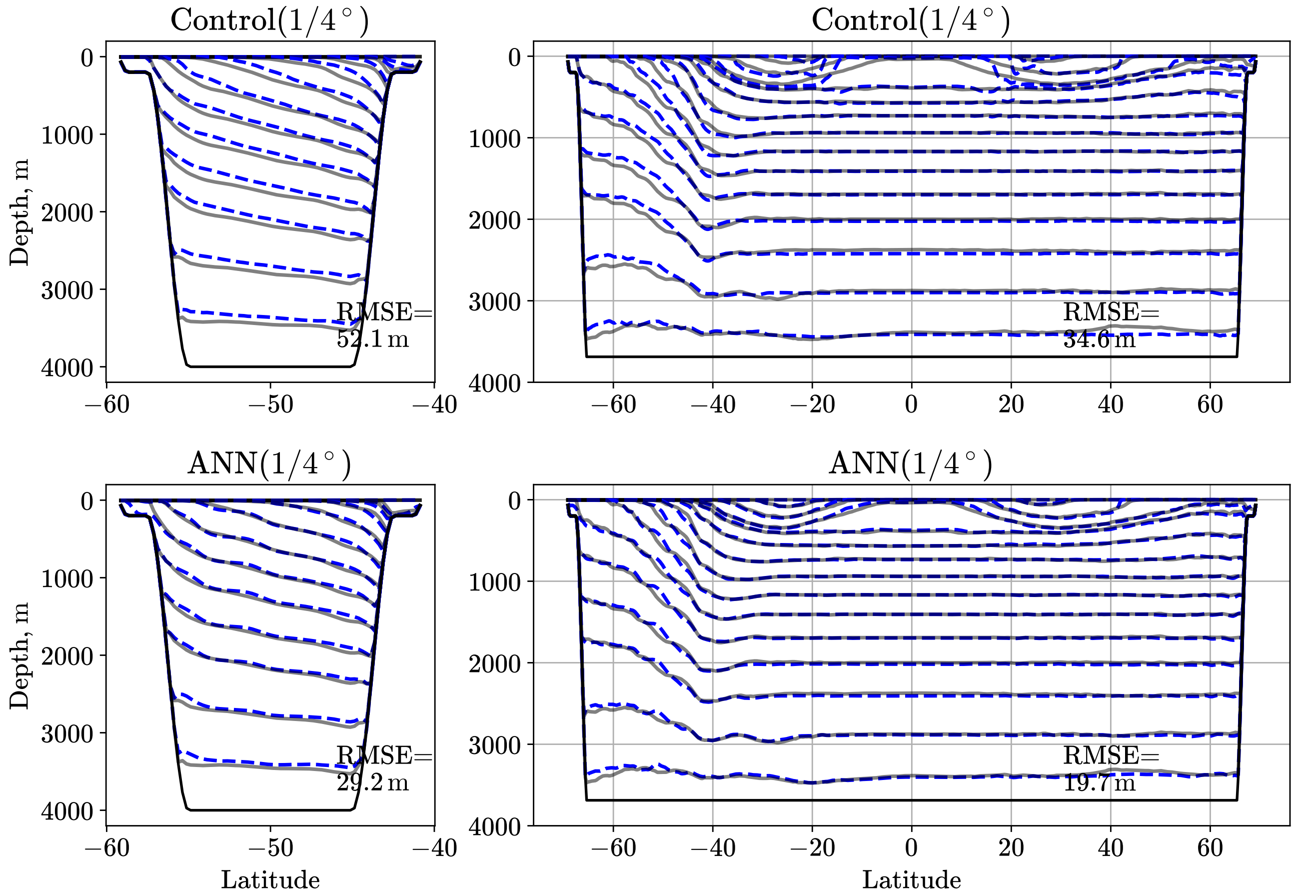


**Figure S3.** Online results in idealized configuration NeverWorld2. The 1000-days averaged isopycnal interfaces in the meridional transect of Drake Passage (Longitude 0°E, left column) and at Longitude 45°E. The blue dashed lines show the position of interfaces in the coarse-resolution (1/4°) experiment, and the gray lines show the interfaces of the high-resolution model 1/32°. The root mean squared errors (RMSE) between coarse and high-resolution models are provided.

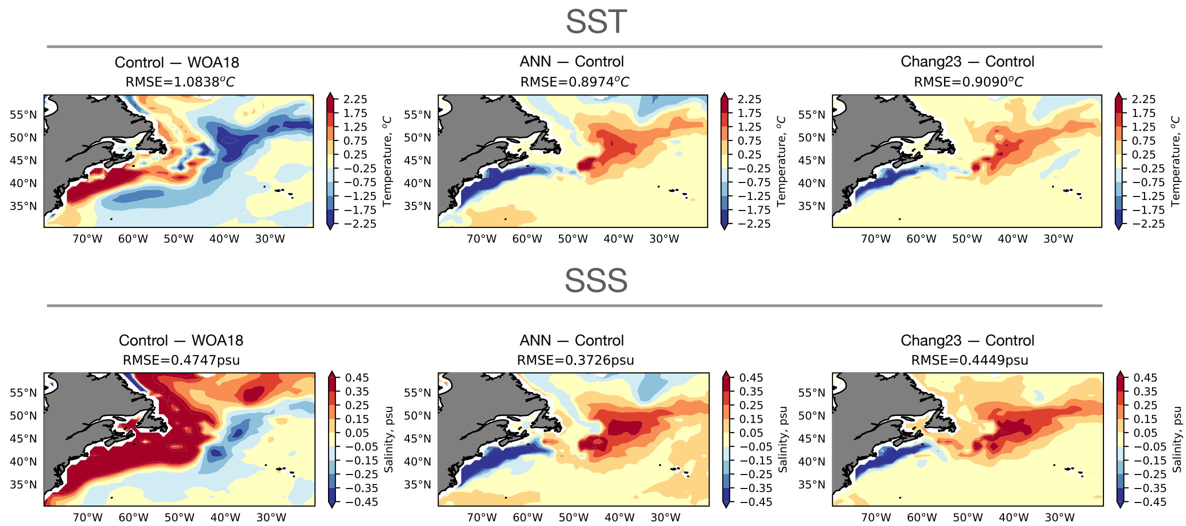


**Figure S4.** Online results in the global ocean-ice model OM4 (Adcroft et al., 2019), North Atlantic region. Comparison of the ANN parameterization to a baseline parameterization tested in Chang et al. (2023). We consider biases in sea surface temperature (SST), sea surface salinity (SSS). Model output is averaged over years 1981-2007. The observational data for SST and SSS is given by the World Ocean Atlas 2018 (WOA18, Locarnini et al. (2018)). Root mean square errors (RMSEs) between simulations and observations are provided.

## References

Adcroft, A., Anderson, W., Balaji, V., Blanton, C., Bushuk, M., Dufour, C. O., ... others (2019). The GFDL global ocean and sea ice model OM4.0: Model description and simulation features. *Journal of Advances in Modeling Earth Systems*, *11*(10), 3167–3211. doi: https://doi.org/10.1029/2019MS001726

Agdestein, S. D., & Sanderse, B. (2025). Discretize first, filter next: Learning divergence-consistent closure models for large-eddy simulation. *Journal of Computational Physics*, *522*, 113577. doi: https://doi.org/10.1016/j.jcp.2024.113577

Chang, C.-Y., Adcroft, A., Zanna, L., Hallberg, R., & Griffies, S. M. (2023). Remote versus local impacts of energy backscatter on the North Atlantic SST biases in a global ocean model. *Geophysical Research Letters*, *50*(21), e2023GL105757. doi: https://doi.org/10.1029/2023GL105757

Griffies, S. M., Winton, M., Anderson, W. G., Benson, R., Delworth, T. L., Dufour, C. O., ... others (2015). Impacts on ocean heat from transient mesoscale eddies in a hierarchy of climate models. *Journal of Climate*, *28*(3), 952–977. doi: https://doi.org/10.1175/JCLI-D-14-00353.1

Grooms, I., Loose, N., Abernathey, R., Steinberg, J., Bachman, S. D., Marques, G. M., ... Yankovsky, E. (2021). Diffusion-based smoothers for spatial filtering of gridded geophysical data. *Journal of Advances in Modeling Earth Systems*, *13*(9), e2021MS002552. doi: https://doi.org/10.1029/2021MS002552

Guillaumin, A. P., & Zanna, L. (2021). Stochastic-deep learning parameterization of ocean momentum forcing. *Journal of Advances in Modeling Earth Systems*, *13*(9), e2021MS002534.

doi: https://doi.org/10.1029/2021MS002534

Gultekin, C., Subel, A., Zhang, C., Leibovich, M., Perezhogin, P., Adcroft, A., … Zanna, L. (2024). An analysis of deep learning parameterizations for ocean subgrid eddy forcing. *arXiv preprint arXiv:2411.06604*. doi: https://doi.org/10.48550/arXiv.2411.06604

Leith, C. (1996). Stochastic models of chaotic systems. *Physica D: Nonlinear Phenomena*, *98*(2-4), 481–491. doi: https://doi.org/10.1016/0167-2789(96)00107-8

Locarnini, M., Mishonov, A., Baranova, O., Boyer, T., Zweng, M., Garcia, H., … others (2018). World ocean atlas 2018, volume 1: Temperature.

Loose, N., Abernathey, R., Grooms, I., Busecke, J., Guillaumin, A., Yankovsky, E., … others (2022). GCM-filters: A Python package for diffusion-based spatial filtering of gridded data. *Journal of Open Source Software*, *7*(70).

Marques, G. M., Loose, N., Yankovsky, E., Steinberg, J. M., Chang, C.-Y., Bhamidipati, N., … others (2022). NeverWorld2: An idealized model hierarchy to investigate ocean mesoscale eddies across resolutions. *Geoscientific Model Development*, *15*(17), 6567–6579. doi: https://doi.org/10.5194/gmd-15-6567-2022

Perezhogin, P., Balakrishna, A., & Agrawal, R. (2024). Large eddy simulation of ocean mesoscale eddies. In *Proceedings of the Summer Program 2024, Center for Turbulence Research, Stanford University* (p. 507-516). Retrieved from `https://arxiv.org/abs/2501.05357`

Perezhogin, P., & Glazunov, A. (2023). Subgrid parameterizations of ocean mesoscale eddies based on Germano decomposition. *Journal of Advances in Modeling Earth Systems*, *15*(10). doi: https://doi.org/10.1029/2023ms003771

Perezhogin, P., Zhang, C., Adcroft, A., Fernandez-Granda, C., & Zanna, L. (2024). A stable implementation of a data-driven scale-aware mesoscale parameterization. *Journal of Advances in Modeling Earth Systems*, *16*(10), e2023MS004104. doi: https://doi.org/10.1029/2023MS004104

Prakash, A., Jansen, K. E., & Evans, J. A. (2022). Invariant data-driven subgrid stress modeling in the strain-rate eigenframe for large eddy simulation. *Computer Methods in Applied Mechanics and Engineering*, *399*, 115457. doi: https://doi.org/10.1016/j.cma.2022.115457

Sane, A., Reichl, B. G., Adcroft, A., & Zanna, L. (2023). Parameterizing vertical mixing coefficients in the ocean surface boundary layer using neural networks. *Journal of Advances in Modeling Earth Systems*, *15*(10), e2023MS003890. doi: https://doi.org/10.1029/2023MS003890

Smagorinsky, J. (1963). General circulation experiments with the primitive equations: I. the basic experiment. *Monthly weather review*, *91*(3), 99–164. doi: https://doi.org/10.1175/1520-0493(1963)091%3C0099:GCEWTP%3E2.3.CO;2

Srinivasan, K., Chekroun, M. D., & McWilliams, J. C. (2024). Turbulence closure with small, local neural networks: Forced two-dimensional and $\beta$-plane flows. *Journal of Advances in Modeling Earth Systems*, *16*(4), e2023MS003795. doi: https://doi.org/10.1029/2023MS003795

Yankovsky, E., Bachman, S., Smith, K. S., & Zanna, L. (2024). Vertical structure and energetic constraints for a backscatter parameterization of ocean mesoscale eddies. *Journal of Advances in Modeling Earth Systems*, *16*(7), e2023MS004093. doi: https://doi.org/10.1029/2023MS004093

Zanna, L., & Bolton, T. (2020). Data-driven equation discovery of ocean mesoscale closures. *Geophysical Research Letters*, *47*(17), e2020GL088376. doi: https://doi.org/10.1029/

2020GL088376

Zhang, C., Perezhogin, P., Adcroft, A., & Zanna, L. (2024). Addressing out-of-sample issues in multi-layer convolutional neural-network parameterization of mesoscale eddies applied near coastlines. *arXiv preprint arXiv:2411.01138*. doi: https://arxiv.org/abs/2411.01138